Correction of Dual-PRF Doppler Velocity Outliers in the Presence of Aliasing

PATRICIA ALTUBE

Meteorological Service of Catalonia, and Department of Astronomy and Meteorology, University of Barcelona, Barcelona, Spain

JOAN BECH

Department of Astronomy and Meteorology, University of Barcelona, Barcelona, Spain

ORIOL ARGEMÍ, TOMEU RIGO, AND NICOLAU PINEDA

Meteorological Service of Catalonia, Barcelona, Spain

SCOTT COLLIS AND JONATHAN HELMUS

Environmental Science Division, Argonne National Laboratory, Argonne, Illinois

(Manuscript received 18 March 2016, in final form 24 February 2017)

ABSTRACT

In Doppler weather radars, the presence of unfolding errors or outliers is a well-known quality issue for radial velocity fields estimated using the dual–pulse repetition frequency (PRF) technique. Postprocessing methods have been developed to correct dual-PRF outliers, but these need prior application of a dealiasing algorithm for an adequate correction. This paper presents an alternative procedure based on circular statistics that corrects dual-PRF errors in the presence of extended Nyquist aliasing. The correction potential of the proposed method is quantitatively tested by means of velocity field simulations and is exemplified in the application to real cases, including severe storm events. The comparison with two other existing correction methods indicates an improved performance in the correction of clustered outliers. The technique proposed is well suited for real-time applications requiring high-quality Doppler radar velocity fields, such as wind shear and mesocyclone detection algorithms, or assimilation in numerical weather prediction models.

1. Introduction

High-quality weather radar Doppler velocity data are essential for automated real-time severe weather detection algorithms (Stumpf et al. 1998; Mitchell et al. 1998; Smith et al. 2004) for assimilation in numerical weather prediction models and nowcasting systems (Sun and Crook 2001; Stensrud et al. 2009; Pierce et al. 2012) and for building climatologies from archived radar data as described in Bellon and Zawadzki (2003), Miller et al. (2013), and Wapler et al. (2016), where multiyear datasets are used to derive specific statistics of the characteristics of thunderstorm mesocyclones. Pulsed Doppler radars estimate the radial velocity of the scattering targets v based on the phase shift between consecutive backscattered pulses. The maximum measurable phase shift between pulses is $\pm\pi$, which poses a limit to the maximum radial velocity that the radar can unambiguously measure. This is known as the Nyquist velocity or aliasing velocity V_a. If scatterers move faster than V_a, then aliasing occurs and the radar estimated velocity is given folded back within the $\pm V_a$ interval, differing from the actual velocity in an integer number of $2V_a$ (Doviak and Zrnić 2006).

The correction of aliased Doppler velocities has historically been the focus of a number of postprocessing algorithms (e.g., Ray and Ziegler 1977; Miller et al. 1986; Bergen and Albers 1988; Eilts and Smith 1990; Jing and Wiener 1993; James and Houze 2001; Haase and Landelius 2004; Xu et al. 2011). An alternative to postprocessing dealiasing is to minimize the aliasing by extending the unambiguous velocity at the processing level. For a fixed radar wavelength, the Nyquist velocity can be extended by increasing the pulse repetition

Corresponding author: Patricia Altube, paltube@meteo.cat; patriciaaltube@gmail.com

DOI: 10.1175/JTECH-D-16-0065.1

frequency (PRF). However, the choice of the PRF involves a trade-off between the Nyquist velocity and the maximum unambiguous range measurable by the radar. Range ambiguities can be mitigated using phase-coding schemes to assign overlaid echoes to the correct range (Sachidananda and Zrnić 1999; Frush et al. 2002). Conversely, extending the Nyquist velocity can be achieved by processing pulses at multiple PRFs, conventionally through the implementation of either staggered multiple-PRT (Sirmans et al. 1976; Torres et al. 2004; Cho 2005; Tabary et al. 2006) techniques or the batch-mode dual-PRF technique (Dazhang et al. 1984). The nonuniform sampling applied in the staggered-PRT schemes hampers the spectral processing involved in traditional clutter-filtering algorithms (Banjanin and Zrnić 1991; Sachidananda and Zrnić 2000). Consequently, the batch-mode dual-PRF strategy has often been chosen for operational use over the staggered schemes and is commonly available in commercial weather radar processors.

In the dual-PRF technique, contiguous atmospheric volumes are probed at two different PRFs and the two resulting velocity estimates are further processed to dealias the velocity within an extended Nyquist interval. The unfolding procedure assumes that the two estimates correspond to the same velocity but, in practice, the assumption may be violated by different factors, such as the presence of high azimuthal shear or due to the uncertainty of the estimates. This leads to an increased dealiasing failure and results in the unfolding mistakes or outliers characteristic of the dual-PRF radial velocity images (Jorgensen et al. 2000; May 2001).

In the present work, a postprocessing algorithm for identification and correction of dual-PRF outliers is presented. The methodology starts by transforming the dual-PRF velocities in radar imagery to angles in a phase space, as discussed by Bharadwaj et al. (2010) for dual-PRT processing. Whereas both techniques use phase space instead of velocity space, the approach used in Bharadwaj et al. (2010) filters all gates regardless of whether or not they are erroneous. In the technique presented here, separate detection and filtering steps are used, such that only the gates deemed erroneous are modified. The technique presented here also uses the phase space differently by first scaling data from different PRFs in different ways and then performing PRF-specific averages from which the presence of velocity outliers can be robustly determined. In particular, for each gate in the image, a mean reference phase is calculated from the phases of the gates in the immediate neighborhood using circular (or directional) statistics (Fisher 1993). The comparison of the phase of the target gate with the calculated mean reference phase allows for identification of outliers. In the computation of the reference phase, the property of angles to wrap around is exploited in order to minimize the bias introduced in the mean by the presence of dual-PRF outliers in the neighborhood. Working in phase space also ensures that the identification process is not affected by the presence of aliasing for extended Nyquist velocities in the target gate nor in the neighboring gates. Once the outlying gates have been identified, the correction of their velocities is carried back to the velocity space. In contrast to existing dual-PRF correction techniques (Joe and May 2003; Holleman and Beekhuis 2003), the proposed methodology can be employed without prior application of extended dealiasing algorithms. This is of particular importance because some of the dealiasing techniques may erroneously correct dual-PRF outliers (see, e.g., Bergen and Albers 1988; Haase and Landelius 2004). Therefore, this characteristic offers increased flexibility for the design of Doppler velocity quality control procedures.

The objectives of this study are to evaluate the performance of the proposed algorithm under simulated conditions in comparison with two existing weather radar dual-PRF correction techniques in order to prove its increased correction potential and to discover its limitations. The ability of the methodology to improve the quality of real dual-PRF data is exemplified through the application to velocity images corresponding to three severe weather events.

2. Dual-PRF technique

The batch-mode dual-PRF scanning technique consists in sending a pulse train at fixed PRF followed by another pulse train with a different PRF (Dazhang et al. 1984). With this procedure, any two gates (resolution volume units) contiguous in the scanning direction are probed, each at a different PRF. In the considerations henceforth, we assume that the ratio of the two PRFs is chosen as a function of an integer dual-PRF factor N in the form

$$\frac{\mathrm{PRF}_h}{\mathrm{PRF}_l} = \frac{V_{ah}}{V_{al}} = \frac{N+1}{N}, \tag{1}$$

where V_{ah} and V_{al} are the Nyquist velocities corresponding to the high and low PRF, respectively. The choice of a PRF ratio in the form given in Eq. (1) ensures that $(N+1)$ and N are coprime integers and that the maximum extension of the unambiguous velocity interval is achieved with the dual-PRF technique (Torres et al. 2004). Commonly used N factors are 2, 3, and 4 (May 2001; Jorgensen et al. 2000; Vaisala 2014).

The phase shift θ_h observed in a gate scanned at the high PRF corresponds to a radial velocity estimate v_h that is given within the $\pm V_{ah}$ Nyquist interval. Similarly, the phase shift θ_l for a gate scanned at the low PRF corresponds to a v_l estimate given within the $\pm V_{al}$ Nyquist interval. The main idea of the dual-PRF procedure is that the velocity of any gate can be dealiased in an extended Nyquist interval $\pm V_{ae}$ using the Doppler information retrieved for the contiguous gate, which has been scanned at a different PRF. Assuming that the "actual" velocity of the scatterers is the same in the two contiguous gates, their corresponding θ_h and θ_l are combined in order to derive a dealiased velocity estimate $\hat{v}_e$ for the target gate (cf. Doviak and Zrnić 2006):

$$\hat{v}_e = \frac{V_{ae}}{\pi}(\theta_l - \theta_h)_{\min}, \tag{2}$$

where the "min" subindex indicates that the smallest angular difference—that is, the modular distance $\min[(\theta_l - \theta_h)\mathrm{mod}2\pi, (\theta_h - \theta_l)\mathrm{mod}2\pi]$—is computed. The corresponding extended Nyquist velocity is given by (cf. Dazhang et al. 1984; Torres et al. 2004)

$$V_{ae} = NV_{ah} = (N+1)V_{al}. \tag{3}$$

After Eq. (2), the error of $\hat{v}_e$ is amplified by the propagation of the errors of the two estimated phase shifts (Jorgensen et al. 2000; Holleman and Beekhuis 2003; Torres et al. 2004). Therefore, in practice, $\hat{v}_e$ is used only to determine the number of folds (n_h or n_l) the originally estimated velocity (v_h or v_l) has undergone within its corresponding Nyquist interval (V_{ah} or V_{al}) depending on whether the target gate has been scanned at the high or low PRF. Then, this number of folds is used to dealias the original velocity so that the standard deviation of the final (dealiased) dual-PRF velocity estimate v_e is only that of the original velocity,

$$v_{eh} = v_h + 2n_h V_{ah}, \tag{4}$$

if the target gate has been scanned at the PRF_h, and

$$v_{el} = v_l + 2n_l V_{al} \tag{5}$$

if the target gate has been scanned at the PRF_l.

Dual-PRF unfolding errors

As explained in Joe and May (2003), dual-PRF unfolding errors occur if the main assumption of the dual-PRF technique is violated, when the difference between the *true* velocities of adjacent gates exceeds a certain threshold,

$$|v_i - v_{i-1}| > \frac{V_{ae}}{N(N+1)} \equiv \Delta v_{\max}. \tag{6}$$

If this inequality is fulfilled, then the $\hat{v}_e$ estimate in Eq. (2) will be biased, and the derived unfolding factor n_h or n_l will be incorrect, differing from the correct factor in an integer number m_h or m_l,

$$\begin{aligned} \mathrm{PRF}_h{:}\, n_h &= n_h^{\mathrm{cor}} + m_h, \\ \mathrm{PRF}_l{:}\, n_l &= n_l^{\mathrm{cor}} + m_l. \end{aligned} \tag{7}$$

Note that the correction factors can take integer values in the intervals $m_h \in (-N, N)$ and $m_l \in [-(N+1), (N+1)]$ and that $m_{h,l} = 0$ indicates that the estimated unfolding factor is correct. When the unfolding factor is incorrect—that is, when $m_h \neq 0$ or $m_l \neq 0$—the dual-PRF velocity estimate for the corresponding gate will also be incorrect, constituting a dual-PRF outlier. According to Eqs. (4), (5), and (7), such an outlier gate will display a dual-PRF velocity that is biased from the correct velocity by either m_h or m_l high or low Nyquist intervals, depending on the PRF at which the gate has been scanned,

$$\begin{aligned} \mathrm{PRF}_h{:}\, v_{eh} &= v_e^{\mathrm{cor}} + 2m_h V_{ah}, \\ \mathrm{PRF}_h{:}\, v_{eh} &= v_e^{\mathrm{cor}} + 2m_h V_{ah}. \end{aligned} \tag{8}$$

Gate-to-gate velocity differences leading to dual-PRF unfolding errors, as required by Eq. (6), arise in regions where the estimated spectral width is large, due to wind shear, turbulence, and/or a low quality of the velocity estimates (see, e.g., Holleman and Beekhuis 2003). Consequently, velocity outliers may appear speckle-wise in isolated gates, generally as a result of random errors in the velocity estimates or systematically clustered together in areas of strong shear or turbulence, or where the quality of the received signal is low. In the present work, we have defined a cluster of dual-PRF outliers as a group of at least four connected outlying gates. Examples of these characteristic dual-PRF unfolding errors in a real-case radial velocity PPI field are indicated in Fig. 1 for the La Miranda radar, located in the northeastern Iberian Peninsula.

The incidence of the outliers is also conditioned by the value of the threshold on the right-hand side of Eq. (6), that is, $\Delta v_{\max}$. For a fixed value of the high PRF, which determines the maximum unambiguous range, the choice of N involves a trade-off between the maximum extension of the Nyquist velocity in Eq. (3) and $\Delta v_{\max}$. For instance, the choice of a high N allows for a large extension of the Nyquist velocity V_{ae} but increases the probability of getting dual-PRF unfolding errors due to a lower $\Delta v_{\max}$. It is therefore a

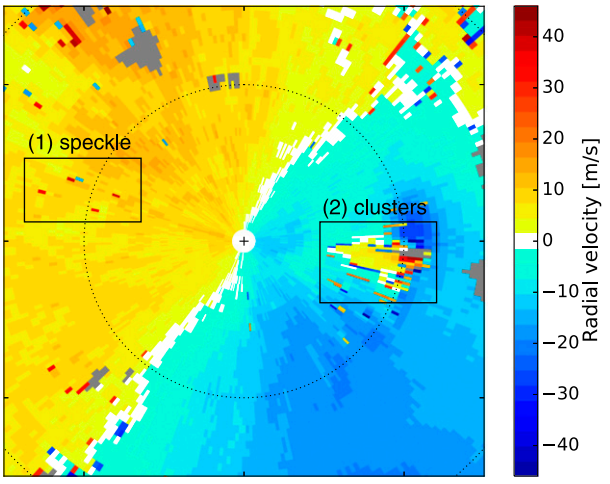

FIG. 1. Example of a base level (0.6°) PPI scan from the La Miranda radar in Catalonia (NE of the Iberian Peninsula) showing dual-PRF radial velocity at 0300 UTC 2 Nov 2008. The PRF ratio of the scan is of 1150/862 Hz, corresponding to a dual-PRF factor of $N = 3$ and an extended Nyquist velocity of $V_{ae} = 45.9\,\mathrm{m\,s^{-1}}$. Black rectangles indicate 1) an area of specklelike dual-PRF outliers and 2) an area of dual-PRF outliers clustered within a highly sheared structure, associated with a severe thunderstorm (Bech et al. 2011). Gates with a nonvalid velocity value are gray, and the dotted ring indicates the 60-km range from radar.

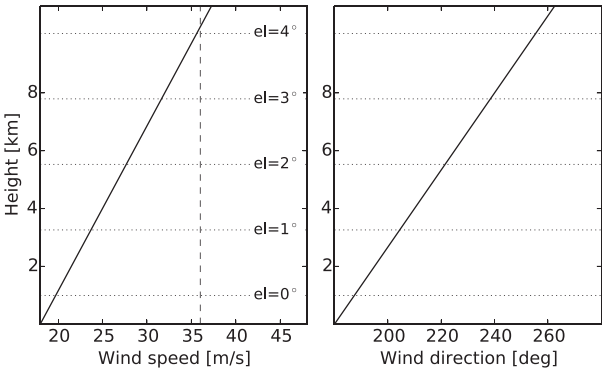

FIG. 2. (left) Wind speed and (right) wind direction vertical profiles of the wind field used for simulation of dual-PRF Doppler velocity volumes. Maximum height of the radar beam axis for the simulated PPI elevations within the volumes (dotted horizontal lines). Term $V_{ae} = 36\,\mathrm{m\,s^{-1}}$ (dashed vertical line).

relevant requirement that a dual-PRF outlier correction procedure performs efficiently in the presence of a high number of outliers while allowing the application of a complementary procedure that corrects aliasing within the $\pm V_{ae}$ interval [called extended Nyquist aliasing, after the terminology employed in WMO (2008, II.9-1–11.9-30)].

3. Simulation of dual-PRF velocity fields

In the present work we will present a technique for the identification and correction of dual-PRF outliers in weather radar velocity imagery. The main strengths of the technique are its robustness in the correction of clustered outliers and that it can be directly applied to dual-PRF velocity images that present extended Nyquist aliasing. To test these qualities for the new technique and for two existing correction techniques, we have simulated a series of dual-PRF velocity fields. Following Brown and Wood (2007), first we have constructed radial velocity fields based on analytical functions representing vertical profiles of a horizontally homogeneous wind field. Then, from each of these radial velocity fields we have derived the following two radar PPI fields of interest:

1) A single-PRF velocity field computed by folding the velocities into a Nyquist interval of $\pm 36\,\mathrm{m\,s^{-1}}$, which constitutes the *reference* field for quantifying the outlier correction ability of the three techniques under study.
2) A dual-PRF radial velocity field computed by folding the velocities in alternate radials into Nyquist intervals of $\pm 12\,\mathrm{m\,s^{-1}}$ (V_{ah}) and $\pm 9\,\mathrm{m\,s^{-1}}$ (V_{al}), corresponding to $N = 3$. The resulting velocities are unfolded within $V_{ae} = 36\,\mathrm{m\,s^{-1}}$ using the dual-PRF technique (section 2).

Figure 2 displays the speed and direction profiles of the first horizontal wind field used in the study. We have generated simulations for a C-band radar of 5-cm wavelength performing PPI scans at five different elevations: 0°, 1°, 2°, 3°, and 4°. In the simulation process, we assume the beamwidth of the radar to be negligible and we compute three wind vector components (u, v, and $w = 0$) for each point of the simulation grid from the corresponding height in the wind profile. The PPI simulation grid has a resolution of 1 km in range and 1° in azimuth, and the minimum and maximum ranges are 2 and 130 km, respectively. After extracting the radial velocity component from the wind vectors, we have also added Gaussian random noise with fixed standard deviation to each radial velocity value. We have computed a series of volumes corresponding to radial velocities with standard deviations that range from 0.1 to $3.0\,\mathrm{m\,s^{-1}}$ in $0.1\,\mathrm{m\,s^{-1}}$ steps. The simulations for the profile shown in Fig. 2 are free of extended aliasing and make up the dual-PRF reference volume for the statistical quantification of the outlier correction performance.

Finally, we have analogously simulated the reference single-PRF and the dual-PRF velocity fields at 4° elevation from the second wind profile shown in Fig. 3. From this second profile a single case is simulated with a Gaussian random noise of $1\,\mathrm{m\,s^{-1}}$ standard

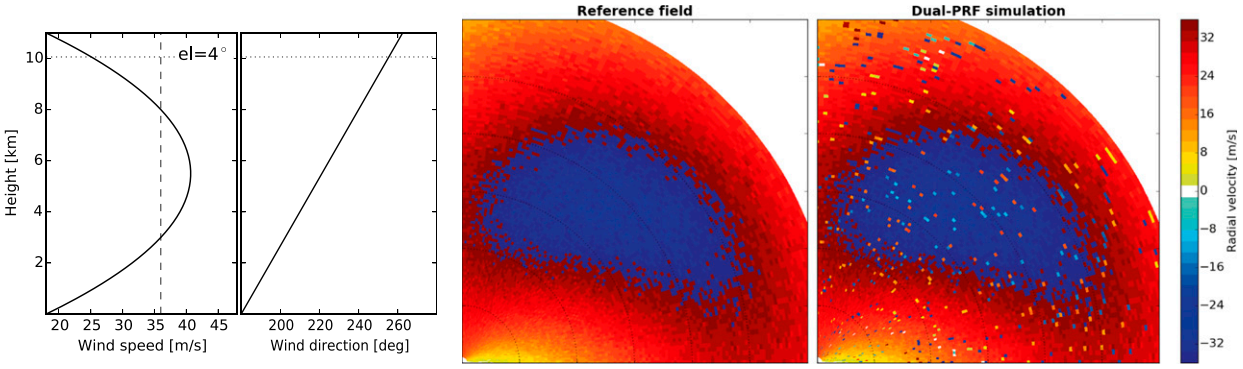

FIG. 3. Example of simulated Doppler velocity fields that present extended Nyquist aliasing: (left) wind speed and wind direction vertical profiles of the wind field used for the simulation and (right) simulated reference radial velocity field and simulated dual-PRF velocity field (zoomed into the upper-right region of the fields). Dual-PRF field has been generated using $N = 3$ and $V_{ae} = 36\ \mathrm{m\,s^{-1}}$. Dotted range rings drawn in the radial velocity fields indicate 20-km intervals.

deviation. As displayed in Fig. 3, the simulated fields in this case present extended aliasing and have been used to qualitatively analyze the performance of the correction techniques in the edges of the aliased regions.

4. Correction of dual-PRF unfolding errors

In this section we present a new postprocessing technique for correcting dual-PRF unfolding errors. This new technique arises from the analysis of two popular correction techniques proposed in the literature. The two techniques studied rely on the continuity of the velocity field and use statistical image processing methods to identify dual-PRF unfolding errors, attending to their outlier characteristics. More precisely, a gate-by-gate analysis of the radial velocity image identifies outlying gates by comparing their velocity with a reference statistic calculated for the gates in their neighborhood: either the mean velocity (*mean* technique; Joe and May 2003) or the median velocity (*median* technique; Holleman and Beekhuis 2003; Cho 2005). The latter is related to the dual-PRF outlier detection technique by Holleman and Beekhuis (2003) and should not be confused with the smoothing median filter commonly applied in image processing.

In the mean and median techniques, the reference statistics are calculated directly from the dual-PRF velocities. When extended Nyquist aliasing is present, the velocity of nonaliased gates may be very different from the local mean or median velocity when there are aliased gates in the neighborhood. Consequently, these gates may be incorrectly identified as dual-PRF outliers. As pointed out in Holleman and Beekhuis (2003), for the correct performance of these dual-PRF correction techniques an extended dealiasing algorithm has to be applied in advance.

The correction of the identified outliers in the mean and median techniques consists of trying all possible unfolding factors [the $m_{h/l}$ integer in Eq. (8)] to determine the one that yields the minimum deviation from the mean or median velocity in the neighborhood. When the PRF at which the outlying gate has been scanned is unknown, all the possible unfolding factors for the low and high PRFs need to be tried (Joe and May 2003). In turn, when the PRF of the target gate is known, this procedure is faster and more robust. However, as described in Holleman and Beekhuis (2003), as long as dual-PRF outliers are present, it is possible to perform a statistical analysis of the velocity estimates to determine in advance which PRF corresponds to each radial.

New postprocessing technique

The new correction procedure proposed is a postprocessing technique that, as the techniques described above, uses local statistics to identify dual-PRF unfolding errors. However, the statistics applied in this case are circular and work on the phase space instead of the velocity space. In particular, the reference velocity for identifying the outliers is derived from the mean phase in the neighborhood. This mean phase is calculated circularly, so it considers the minimum angular differences (modular differences) between the phases of the surrounding gates. As detailed in the following, the proposed technique—the *cmean* method—treats outlier identification and correction separately in two differentiated stages.

1) IDENTIFICATION

Term v_e can be expressed as phases α in a circle of radius V_{ae}/π,

$$\alpha = \pi \frac{v_e}{V_{ae}}. \tag{9}$$

From Eq. (8) and using the relation in Eq. (3), we have

$$\begin{aligned} \mathrm{PRF}_h: \alpha_h &= \pi \frac{v_e^{\mathrm{cor}}}{V_{ae}} + 2\pi m_h \frac{V_{ah}}{V_{ae}} = \alpha^{\mathrm{cor}} + 2\pi \frac{m_h}{N}, \\ \mathrm{PRF}_l: \alpha_l &= \pi \frac{v_e^{\mathrm{cor}}}{V_{ae}} + 2\pi m_l \frac{V_{al}}{V_{ae}} = \alpha^{\mathrm{cor}} + 2\pi \frac{m_l}{(N+1)}. \end{aligned} \tag{10}$$

If the relations in Eq. (10) are multiplied by N and $(N+1)$ respectively, then the second term on the right-hand side results in an integer factor of 2π for both the high- and low-PRF cases. Therefore, the following congruences hold:

$$\begin{aligned} \mathrm{PRF}_h: N\alpha_h &\equiv N\alpha^{\mathrm{cor}} (\mathrm{mod}\, 2\pi), \\ \mathrm{PRF}_l: (N+1)\alpha_l &\equiv (N+1)\alpha^{\mathrm{cor}} (\mathrm{mod}\, 2\pi). \end{aligned} \tag{11}$$

In this way, if the circular mean of the scaled phases is computed considering only the neighboring high-PRF gates, then an estimate of $N\alpha_h^{\mathrm{cor}}$ is obtained that will not be biased if outlying gates or gates with extended aliasing are included in the averaged sample. Analogously, the circular mean of the scaled phases of neighboring low-PRF gates will give an unbiased estimate of $(N+1)\alpha_l^{\mathrm{cor}}$.

Based on these ideas, the proposed dual-PRF identification stage is sketched in Fig. 4 and summarized in the following steps:

1) Convert v_e to phases α through multiplication by (π/V_{ae}).
2) Multiply the α phases by N or $(N+1)$, depending on the scanning PRF, to obtain the scaled phases α'.
3) Compute the circular average of the scaled phases in a 5×5 window around each of the gates, separately for low- and high-PRF neighboring gates within the window. This step yields two average phases for each gate, β_l and β_h, which constitute estimators of $(N+1)\alpha^{\mathrm{cor}}$ and $N\alpha^{\mathrm{cor}}$, respectively, given in the base phase interval $[-\pi, \pi]$,

$$\begin{aligned} \mathrm{PRF}_h: \beta_h &= \mathrm{a\,tan2}\left(\frac{1}{M_h} \sum_{j=1}^{M_h} \sin\alpha'_j, \frac{1}{M_h} \sum_{j=1}^{M_h} \cos\alpha'_j \right), \\ \mathrm{PRF}_l: \beta_l &= \mathrm{a\,tan2}\left(\frac{1}{M_l} \sum_{k=1}^{M_l} \sin\alpha'_k, \frac{1}{M_l} \sum_{k=1}^{M_l} \cos\alpha'_k \right), \end{aligned} \tag{12}$$

where the a tan2 function is the two-argument arctangent function that considers the sign of the two arguments in order to compute the arc angle in the appropriate quadrant. The index j runs for all high-PRF gates within the 5×5 window and the index k runs for all low-PRF gates in the same window. The 5×5 size of the filter window is chosen so that a sensible number of both high-PRF and low-PRF estimates are available for calculation of the corresponding circular averages. It is required that at least two high-PRF and two low-PRF gates within the window contain a valid velocity value for calculation of the average. The maximum number of high- and low-PRF gates—that is, M_h and M_l, respectively—within the 5×5 window will be either 10 or 14, depending on the PRF of the central gate.

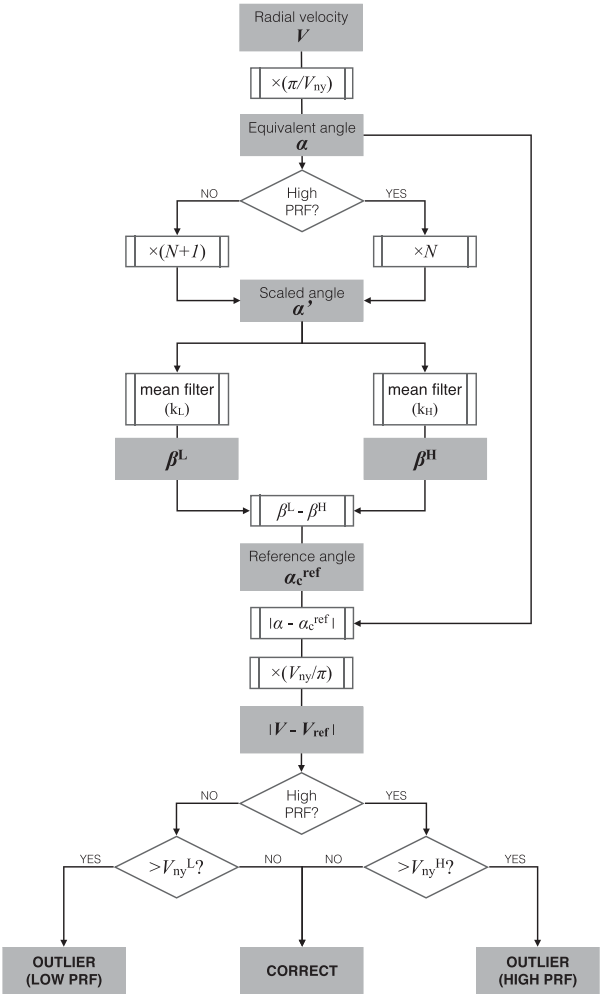

FIG. 4. Flowchart description of the proposed dual-PRF velocity outlier identification procedure using circular statistics.

4) Estimate the correct reference phase α^{ref} from

$$\alpha_{\mathrm{ref}} = \begin{cases} (\beta_l - \beta_h), & \text{if } (\beta_l - \beta_h) \geq 0 \\ (\beta_l - \beta_h) + 2\pi, & \text{otherwise} \end{cases}. \tag{13}$$

5) Calculate the minimum angular difference between the dual-PRF phase and the reference phase for each gate,

$(\alpha - \alpha_{\text{ref}})_{\text{min}}$, and convert this phase difference to a velocity difference through multiplication by (V_{ae}/π).

6) Identify outlying gates as those with a velocity difference greater than their corresponding Nyquist velocity (V_{al} or V_{ah}).

The reference phase estimate is obtained by differencing β_l and β_h, which are averages of scaled phases. Hence, the standard deviation of the reference velocity is amplified by a factor of approximately $\sqrt{(N+1)^2 + N^2}$, when compared to a reference velocity derived from the direct average of the velocities of the neighboring gates. It is also important to note that the reference phase can be unambiguously estimated from this $(\beta_l - \beta_h)$ difference only when the PRF ratio fulfills Eq. (1). For PRF ratios in the form $(N + d)/N$ with $d \neq 1$, additional constraints need to be included in the algorithm because the quantity $1/d(\beta_l - \beta_h)$ would produce d possible reference phases in a $[-\pi, \pi]$ interval.

2) CORRECTION

Once potential dual-PRF outliers have been identified, the next stage corrects them using a procedure similar to that of the median method. The local median velocity in a 5×5 window around the outlier gate is calculated and the deviation of the target gate velocity from this reference is computed for all possible correction factors. The values of the possible correction factors are determined by N and are conditioned by whether the outlier gate has been scanned at high or low PRF [see Joe and May (2003), for an example with $N = 3$]. The correction factor $m_{h/l}$ applied in Eq. (8) is the one that yields the minimum velocity difference. In addition, the following points must be verified:

- Gates that have been labeled as outliers in the identification process are excluded from the calculation of the median.
- Only gates that have been labeled as outliers in the identification process are corrected.
- Only identified outliers that have at least two valid neighbors are corrected.

The first and last requirements have an effect on the number of valid gates available for the calculation, especially when the outliers appear clustered or close to missing value regions, but minimize the probability of an erroneous correction.

5. Analysis of correction techniques

The characteristics of the statistics used by each of the three dual-PRF outlier correction techniques can be qualitatively investigated from the distributions of the local velocity deviation in each case. We have constructed these distributions from the local velocity deviations of each and all the gates in the simulated dual-PRF velocity volumes described in section 3. The local velocity deviation is the difference between the velocity of the target gate and a reference velocity, which is computed differently depending on the correction technique and which is representative of the local velocity field. For the median and mean methods, we have calculated the reference velocity as either the median or the mean velocity of the gates with a nonmissing velocity value in a 3×3 window around the target gate. In the case of the median method, we have also included the central target gate in the calculation as in Holleman and Beekhuis (2003). For the cmean method, the velocity deviations have been calculated following the steps described in section 4a.

Figure 5 shows the distributions of the local velocity deviations for the three correction techniques. In all distributions, the velocity difference has been scaled by the Nyquist interval corresponding to the target gate: $2V_{ah}$ if the gate has been scanned at the PRF_h or $2V_{al}$ if the gate has been scanned at the PRF_l. Note that for the mean and median techniques, the velocity difference is a simple (not modular) distance calculated directly in the velocity space and can take values in the $(-2V_{ae}, 2V_{ae})$ interval. When this interval is scaled, we get $(-N, N)$ for the PRF_h and $[\theta - (N+1), (N+1)]$ for the PRF_l, indicating that when $N = 3$ the peaks can be found at $0, \pm 1, \pm 2$ for the PRF_h and $0, \pm 1, \pm 2, \pm 3$ for the PRF_l [see also section 3.4 in Joe and May (2003)]. This way, the scaled velocity difference is, for the mean and median, an indicator of how many Nyquist intervals the dual-PRF velocity is in error, that is, $m_{l/h}$ in Eq. (8).

As observed in the top panel of Fig. 5, when the median velocity is used as reference for the calculation of the deviation, dual-PRF outliers are clearly identified as those with a deviation greater than the corresponding high- or low-PRF Nyquist velocity (dashed vertical lines). The median is a reliable estimator of the reference velocity when the percentage of outliers in the sample drawn from the neighborhood is below the accepted breakpoint of 50% (Hampel et al. 1986). Consequently, in the identification process a few outliers may be missed and correctly unfolded gates may be erroneously identified as outliers if the number of outlier neighbors is higher than 50%. However, the deviation histogram presents well-defined peaks of limited width at integer multiples of the corresponding Nyquist interval and therefore correctly identified outliers can be accurately corrected based on the median reference velocity.

On the other hand, and as indicated by the results presented in the central panel of Fig. 5, the presence of outliers in the neighborhood has a significative biasing

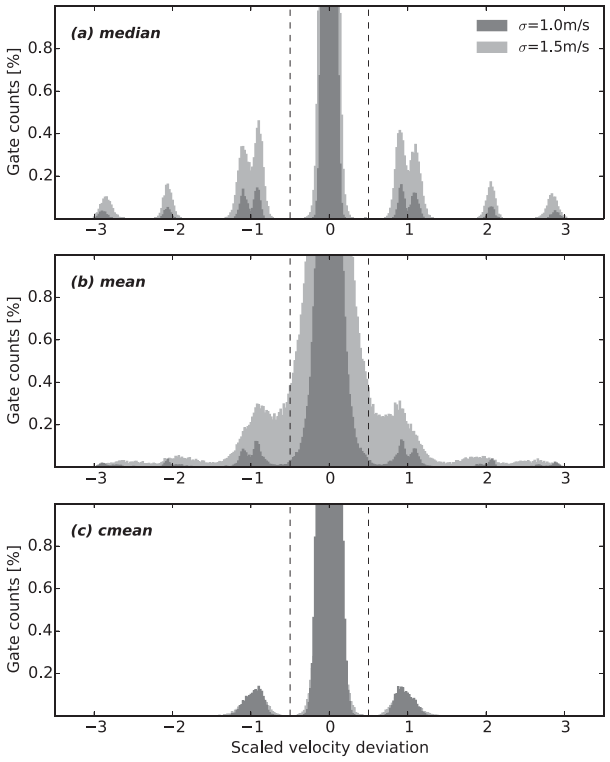

FIG. 5. Histograms of the velocity deviation of each gate from (top) local median velocity, (middle) local mean velocity, and (bottom) local circular mean. Velocity deviation is scaled by the Nyquist interval corresponding to the scanning PRF of the gates. Total number of gates considered is 230 400, encompassing all gates in the simulated dual-PRF velocity fields at five different elevations (0°–4°). The dual-PRF factor is $N = 3$ and the extended Nyquist velocity is $V_{ae} = 36\ \mathrm{m\,s^{-1}}$. Two cases of radial velocity standard deviation are presented: $1.0\ \mathrm{m\,s^{-1}}$ (dark gray) and $1.5\ \mathrm{m\,s^{-1}}$ (light gray). Minimum deviation thresholds identify the dual-PRF outliers (vertical dashed bars).

effect on the reference mean velocity. When the standard deviation of the radial velocities is increased, the number and concentration of dual-PRF outliers increases. As a result, the calculated velocity deviations are highly variable and the large spread of the distribution peaks indicates that 1) misses and false alarms are likely to occur in the identification of outlying gates, especially in the overlapping area for gates with scaled velocity deviations between 0 and ±1 (close to dashed vertical bars) and 2) outlier gates whose scaled deviation lies approximately midway between two integers may be erroneously corrected.

Finally, the distributions for the cmean technique in the bottom panel of Fig. 5 indicate that dual-PRF outliers can be clearly identified as those with a scaled velocity difference beyond the dashed vertical lines. The case of this technique is different because the velocity difference is a modular distance calculated from the phases. This modular distance in phase space can take values only in the $[-\pi, \pi]$ interval. When expressed in the velocity space, the interval transforms into $[-V_{ae}, V_{ae}]$ and after scaling transforms into $[-N/2, N/2]$ for the PRF_h and $[-(N+1)/2, (N+1)/2]$ for the PRF_l. Consequently, the scaled velocity difference is never greater than ±2 (for $N = 3$) and its distribution peaks at ±1. This indicates that the procedure serves to identify the outliers but that the circular mean reference does not give enough information for correction, therefore requiring a correction stage based on velocity statistics instead of phase statistics, as proposed in section 4b.

6. Quantitative performance analysis

In this section we quantitatively assess the performance of the new cmean dual-PRF outlier correction technique in comparison with the existing mean and median techniques. The three correction techniques are applied, in two separate analyses, to the simulated dual-PRF velocity volumes and to a collection of real fields scanned at a single PRF that have been further aliased to dual PRF. In the implementation of the mean technique, we have modified the correction methodology in an analogy to the cmean technique; that is, identified outliers are excluded from the local mean calculations in the correction stage. This two-stage procedure is similar to the extension of the Joe and May (2003) mean method reported in Hengstebeck et al. (2014) and is thought to minimize the erroneous correction of identified outliers pointed out in section 5.

The location of the outliers in the dual-PRF fields and the corresponding correction factor are known by comparison with the reference single-PRF field in each case. This allows us to label the gates separately in the identification and correction stages of the dual-PRF outlier correction techniques in order to quantify the quality improvement brought out by the technique. Figure 6 schematically depicts the gate labeling, classifying them as correct negatives (correctly unfolded gates that have been correctly identified as nonoutliers), false alarms (correct gates erroneously identified/corrected as outliers), misses (outlier gates not identified/corrected), and hits (outlier gates appropriately identified and corrected). To statistically quantify the performance of the dual-PRF correction methods, we use the probability of detection (POD) verification index, analogous to the effectiveness in the present context, and define an efficiency index (EI),

$$\mathrm{POD} = \frac{\mathrm{hits}}{(\mathrm{hits} + \mathrm{misses})} = \frac{\mathrm{hits}}{\mathrm{outlier\ gates}}, \tag{14}$$

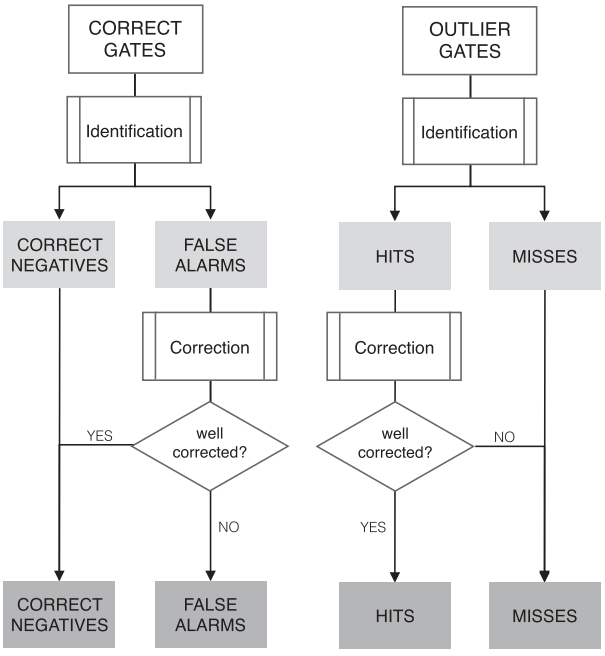

FIG. 6. Labeling process of the velocity field gates, based on the quality of the dual-PRF outlier identification (light gray labels) and correction (dark gray labels).

$$\mathrm{EI} = \frac{\text{hits} - \text{false alarms}}{(\text{hits} + \text{misses})} = \frac{\text{hits} - \text{false alarms}}{\text{outlier gates}}. \quad (15)$$

The EI statistic indicates the fraction of outliers efficiently corrected, accounting for the generation of new outliers by the false alarms. The index traditionally used to quantify the false alarm rate, the probability of false detection (POFD), is not an appropriate statistic for the present analysis because the number of false alarms (and also the number of outliers) is in most cases small relative to the number of correct gates. Instead, the POD − EI difference may be used as an alternative indicator of the false alarm rate.

Dual-PRF velocity fields from simulations

Figure 7 displays the results of the application of the three correction techniques—mean, median, and cmean—to the dual-PRF field with extended aliasing presented in section 3. The panels in Fig. 7 correspond to the northeast region of the field in Fig. 3 and show both the corrected field for each of the correction techniques and the corresponding gate labeling described above. This example shows how the median and mean methods generate false alarms and miss some of the outliers in the boundaries of the aliased region, while the cmean method respects the nonoutlier gates and appropriately corrects the outliers.

The three outlier correction techniques have also been applied to the series of simulated nonaliased dual-PRF velocity volumes. Taking into account that the outliers in the simulated fields arise uniquely as a result of random processes and that the noise distribution is Gaussian with a fixed standard deviation, the fraction of outliers out of the total number of gates depends only on the ratio between the threshold in Eq. (6) and the standard deviation of radial velocities: $\Delta v_{\max}/\sigma$. This result may be derived from the Gaussian cumulative distribution function and $\Delta v_{\max}$, as described in Holleman and Beekhuis (2003). Since the standard deviation of the radial velocities is different for each simulated volume, the performance of the techniques for the different levels of clustering of the outliers can been assessed based on the analysis of the POD and EI verification indexes calculated for the corrected volumes.

The five simulated PPI fields within a volume contain a total of 230 400 gates. The fraction of outliers out of the total gates sampled is displayed in Fig. 8 as a function of the $\Delta v_{\max}/\sigma$ ratio. Figure 8 also shows the fraction of gates with more than four outliers in the immediate neighborhood (within a 3×3 sized window) and the fraction of clustered outliers. The latter accounts for all the outlier gates within a cluster, having defined a cluster as a collection of more than three contiguous outliers. The number of outliers grouped into clusters increases with decreasing $\Delta v_{\max}/\sigma$ ratios. This increase is particularly significant for ratios below 1.8 and when the $\Delta v_{\max}$ threshold equals the standard deviation of the velocity estimates, at which point almost all outliers pertain to a cluster and more than half of the total gates have more than four outliers in their neighborhood.

Figure 9 displays the POD and EI indexes as a function of $\Delta v_{\max}/\sigma$ for the three correction methods. The indexes separately score the identification and correction performance of the methods. From the POD values for the median technique, it is derived that the number of misses in identification increases rapidly for ratios below $\approx$1.6, coinciding with the increase in the fraction of gates surrounded by more than four outliers. In addition, the median POD scores in correction indicate that the percentage of well-corrected outliers drops when the noise level increases. The comparison of POD and EI values leads to a similar conclusion for the false alarm rate. These results are attributed to the increasing concentration of outliers and their biasing effect in the calculation of the local median. In the implementation of this method, identified outliers (hits and false alarms) are not removed in the correction stage and therefore all false alarms in identification remain false alarms after correction, so the EI scores alone do not give additional information. As anticipated in section 5, the number of

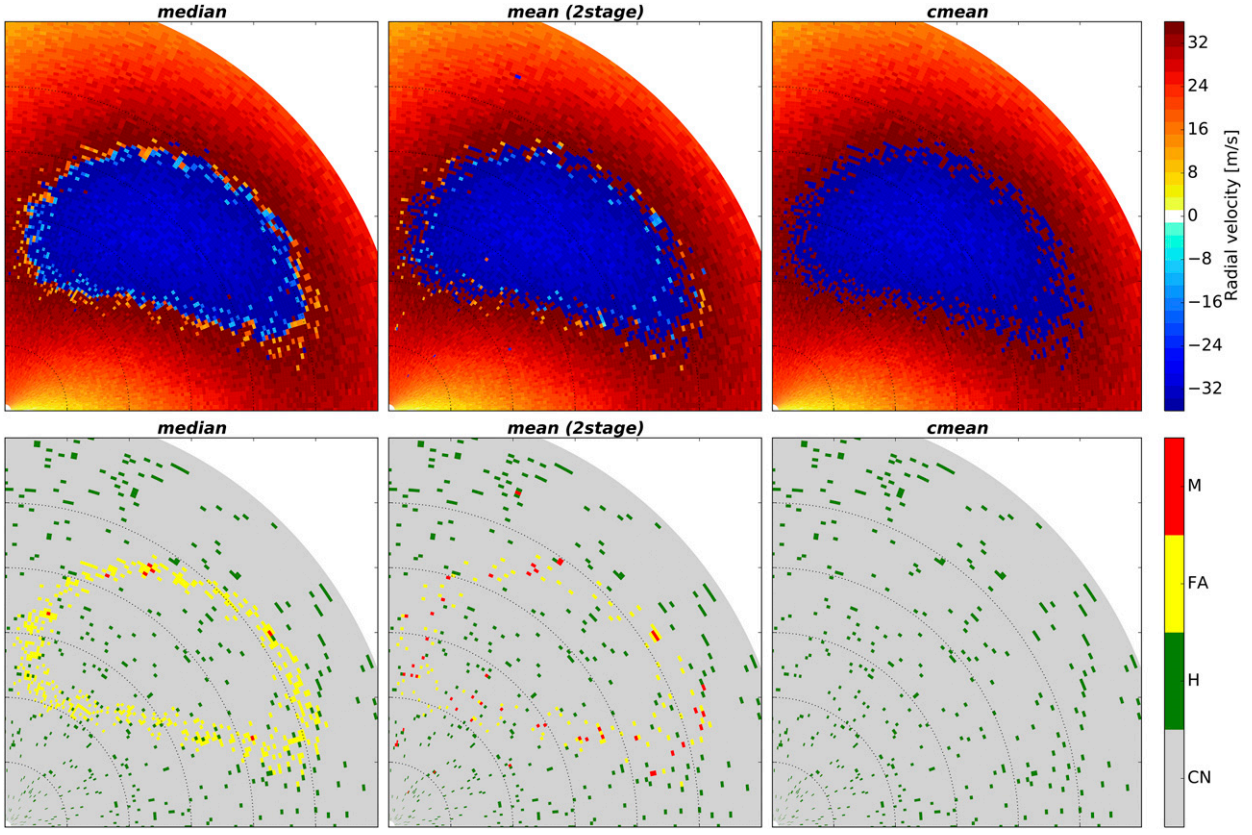

FIG. 7. Comparative results of dual-PRF outlier correction in the presence of extended Nyquist aliasing, by means of the mean, median, and cmean techniques: (top) corrected fields for each of the techniques and (bottom) labeling of each of the gates in the corrected fields as correct negatives (CN), hits (H), false alarms (FA), and misses (M). Original uncorrected dual-PRF field has been simulated at an elevation of 4° from the wind profiles in Fig. 3, with a dual-PRF factor of $N = 3$, an extended Nyquist velocity of 36 m s^{-1}, and a radial velocity standard deviation of 1 m s^{-1}. Dotted range rings indicate 20-km intervals.

misses and false alarms in identification is higher for the mean method. However, the high false alarm rate in identification is somewhat reduced in the correction stage by the removal of the identified outliers. The POD results suggest that the outlier removal requirement in the second stage is able to mitigate the erroneous correction of actual outliers (hits) only for ratios higher than ≈2.5.

As shown in Fig. 8, when $\Delta v_{max}/\sigma \approx 1$, around half of the gates are outliers and around 80% of these outliers are grouped into clusters. The POD values for the cmean method show that this new technique identifies close to 100% of the outliers down to a $\Delta v_{max}/\sigma$ ratio of 1. In turn, the EI values in identification indicate that for ratios below ≈1.6 the cmean method generates a significative number of false alarms. However, practically all these false alarms in identification are left uncorrected and more than 90% of the outliers are properly corrected in the second correction stage. The improvement achieved in the correction stage is attributed to the high hit rate in identification; with the removal of these identified outliers, the bias of the local median velocity reference is minimized and the appropriate correction factor is derived.

7. Application to real cases

The performance of the proposed cmean technique under actual dual-PRF measurement conditions is illustrated in Fig. 10 for velocity images from three different events, recorded by Puig Bernat (PBE), La Miranda (LMI), and Creu del Vent (CDV) C-band radars, located in the Catalonia region of Spain (northeast of the Iberian Peninsula) and operated by the Meteorological Service of Catalonia (SMC). The PBE and CDV radars estimate the radial velocity of the scatterers in dual-PRF mode with a PRF ratio of 1000/750, while the LMI radar scans with a PRF ratio of 1150/862, corresponding to extended Nyquist velocities of 40.0 and 45.9 m s^{-1}, respectively. The raw velocity data provided by these radars are filtered in the processor (Vaisala 2014) by application of a clutter signal ratio (CSR) threshold of 18 dB and a signal quality index (SQI) threshold of 0.35. A detailed

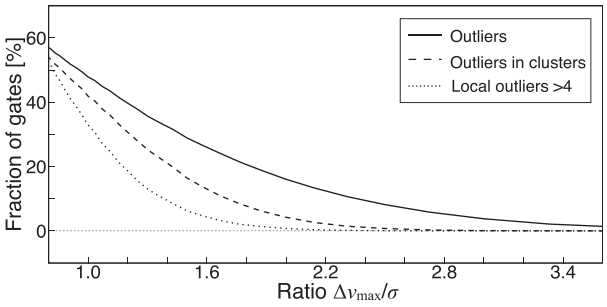

FIG. 8. Fraction of outliers (solid line), fraction of clustered outliers (dashed line), and fraction of gates with more than four outliers in their immediate neighborhood (dotted line) as a function of the $\Delta v_{max}/\sigma$ ratio in simulations of dual-PRF radial velocity fields. Percentages are given based on the total number of gates (230 400), encompassing all gates in the simulated fields at five different elevations (0°, 1°, 2°, 3° and 4°). The dual-PRF factor is $N = 3$ and the extended Nyquist velocity is $V_{ae} = 36\ \mathrm{m\,s^{-1}}$.

description of the SMC radar network and technical characteristics can be found in Bech et al. (2004) and in section 3 in Altube et al. (2015).

The first case studied corresponds to a tornado reported in Bech et al. (2007) and rated F2 on the Fujita scale that took place on 7 September 2005, affecting the Barcelona–El Prat Airport. The image in the upper-left panel of Fig. 10 is a reproduction of Fig. 10 in Bech et al. (2007) and shows the radial velocity field observed by the PBE radar minutes after the tornado crossed the runways of the airport, moving inland on a southeast–northwest track. The correction of the dual-PRF field by means of the cmean method, displayed in the panel immediately below, allows for the clear identification of the couplet associated with the mesocyclone to the east of the radar site.

The second image presented is a snapshot by the LMI radar extracted from the tornadic event that took place between 0000 and 1200 UTC 2 November 2008, and is described in Bech et al. (2011), Pineda et al. (2011), and Roca-Sancho et al. (2014). The velocity image, shown in the upper-middle panel of Fig. 10, is a zoomed-out view of Fig. 1 and corresponds to the time of maximum ground damage (rated as F1 on the Fujita scale) by a thunderstorm microburst on the southern coast of Catalonia. The processing of the raw dual-PRF image by the cmean technique adequately corrects most of the dual-PRF dealiasing errors in a single pass, clarifying the divergent structure of the microburst. Only a few outliers are missed, in particular cases found within zones of high variability in the estimated velocities.

The third case image, in the upper-right panel of Fig. 10, is part of a severe thunderstorm event that produced hailstones with a maximum diameter of 3.5 cm in western Catalonia. The figure displays the velocity field observed by the CDV radar immediately after the time of maximum hail fall. Hours later, the same thunderstorm produced an important flood event in the Val d'Aran valley (northwest of Catalonia). In this case, highly sheared areas in the northwestern portion of the image have been filtered out. These areas are recognizable by the high amount of dual-PRF outliers in their borders. This image also presents two aliased zones, one to the north and a larger one in the south. The cmean procedure corrects the clustered outliers in the borders of filtered out areas while preserving the edges of the zones with global aliasing. It can also be observed that the correction may have a higher failure rate in regions of clustered outliers that are semi-isolated, that is, surrounded by gates with a nonvalid velocity value.

8. Summary and conclusions

The dual-PRF technique is widely used to extend the unambiguous velocity interval within which Doppler weather radars estimate the radial velocity of the scatterers. However, dual-PRF radial velocity images present characteristic unfolding errors or outliers that arise due to the violation of the assumptions involved in the procedure. In the present manuscript, we have analyzed two existing postprocessing techniques that identify and correct dual-PRF outliers by comparing the gate velocity with the mean or median velocity of the surrounding gates. We have shown that these techniques require that a global dealiasing algorithm is run prior to the correction of the outliers and that their performance is limited by the presence of outliers in the surroundings.

From these premises, we have presented a new postprocessing technique to correct dual-PRF outliers. It is similar to the existing techniques; it relies on the continuity of the local field but uses circular statistics and does not need a prior global dealiasing. This new technique is built in two stages that treat the identification and the correction of the outliers separately. In the identification stage, the gate velocities are converted into phases in a circle with a circumference that is twice the extended unambiguous velocity given by the dual-PRF procedure. The statistics to compute the local reference velocities that allow for the identification of the outliers are calculated from these phases instead of directly on the velocities and therefore are not influenced by gates that are globally aliased. The method, as proposed in the present work, requires that the ratio of the high and low PRFs is of the type $(N + 1)/N$ and that the PRF at which each radial has been scanned is known. The latter information is used to devise the identification algorithm in a way that the biasing effect of neighboring outliers in the calculation of the reference velocity is minimized. Working on the

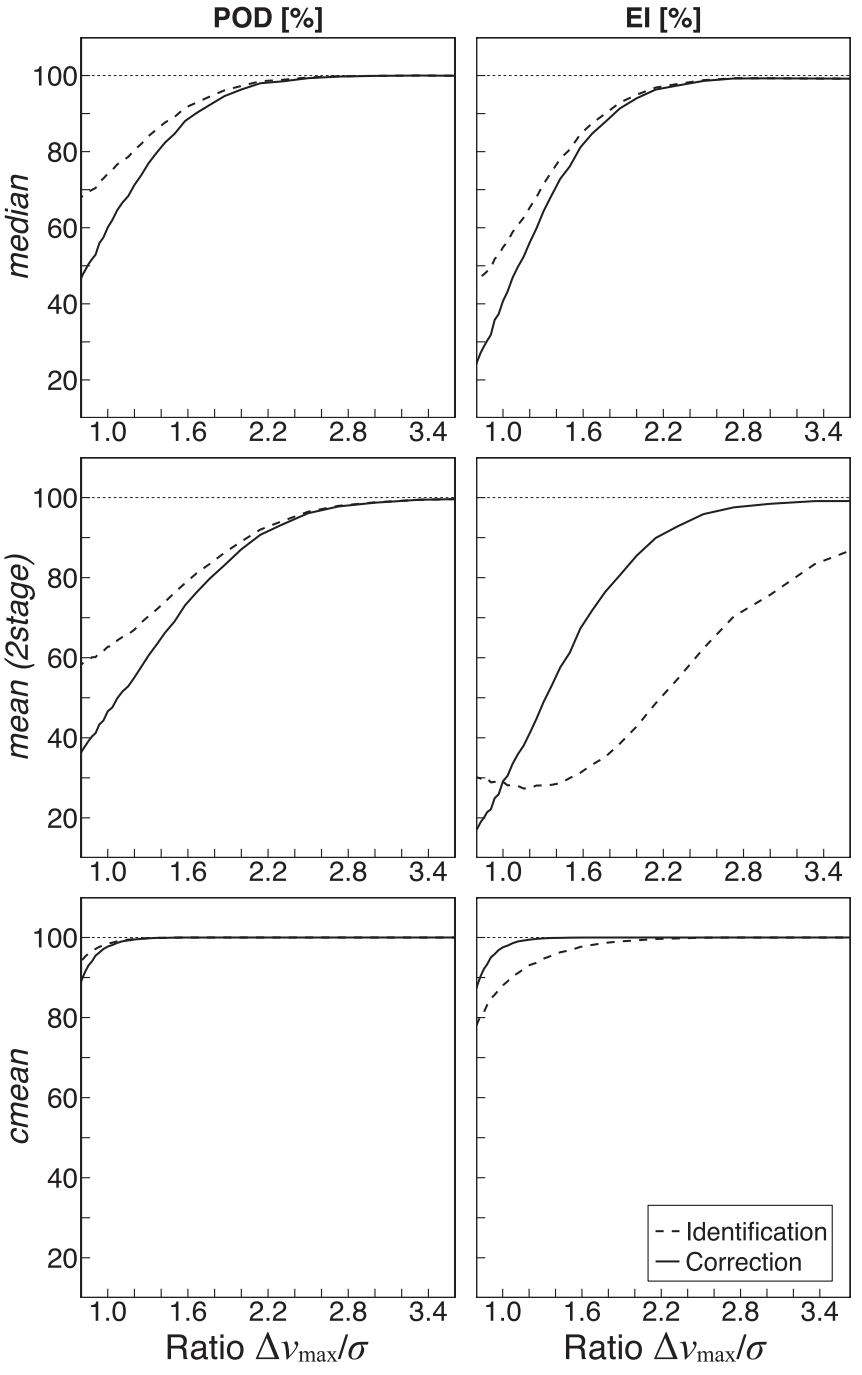

FIG. 9. (left) POD and (right) EI of the (top) median, (middle) mean, and (bottom) cmean dual-PRF correction methods. Indexes are displayed as a function of the $\Delta v_{max}/\sigma$ ratio in the simulations of dual-PRF velocity fields and are calculated separately for the outlier identification (dashed line) and correction (solid line) stages.

circular phase space allows only for the identification of the outliers and hence their correction needs to be carried out in velocity space, after the removal of the surrounding outliers to prevent biases in the correction factors. The methodology used to correct the identified outliers in the second stage is similar to that of the existing post-processing technique based on the local median velocity, which is shown to be a more robust statistic than the mean

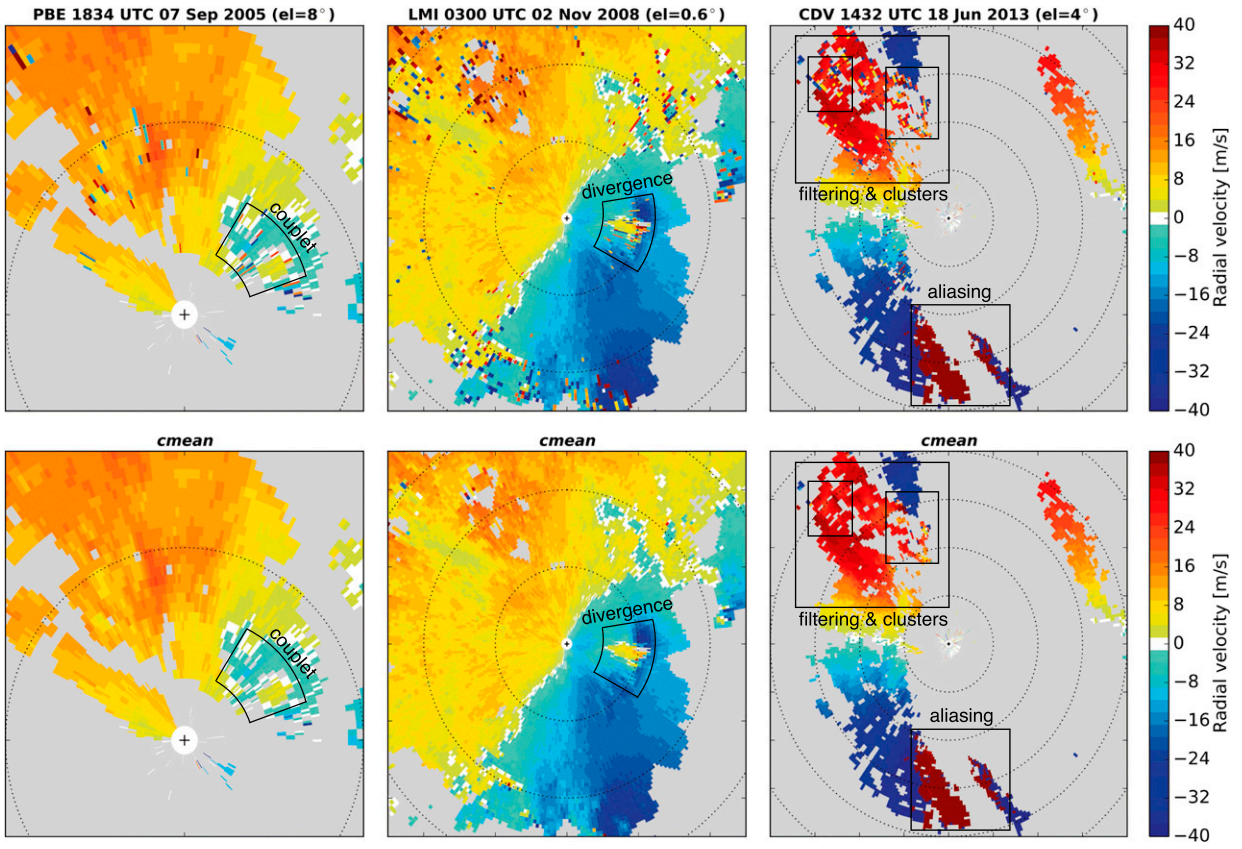

FIG. 10. Correction of real dual-PRF data using the cmean technique. Radial velocity PPI images from (left) the PBE radar at 1834 UTC 7 Sep 2005 at an elevation of 8.0°, (middle) the LMI radar at 0300 UTC 2 Nov 2008 at an elevation of 0.6°, and (bottom) the CDV radar at 1432 UTC 18 Jun 2013 at an elevation of 4.0°. Gates with a nonvalid velocity value are gray, and dotted range rings indicate 20-km intervals.

velocity for the purpose. The removal of outliers with the requirement that at least two surrounding gates have a valid velocity value may in a few cases hamper the correction due to a lack of valid data in the neighborhood.

We have quantitatively assessed the performance of the new technique using simulated dual-PRF fields. The analysis has shown that the proposed method is more effective and efficient in the identification of dual-PRF outliers than the two existing procedures analyzed, denoting a significative improvement when the concentration of outliers is high. This is of particular importance because clusters of dual-PRF outliers are likely to be present in highly sheared areas, which are usually regions of interest when studying severe weather events. On the other hand, all three methods perform similarly in the correction of the identified outliers; however, if the removal of the outliers is applied prior to the correction stage, then the false alarm rate is reduced. It has been shown that in the application to real dual-PRF velocity fields, exemplified through three dual-PRF velocity images corresponding to different severe weather events, the proposed technique satisfactorily corrects the outliers. Under real measurement conditions, it has been noticed that the new algorithm may sporadically miss outliers and probably generate false alarms in areas where the underlying field is highly variable. This is attributed to inaccuracies in the reference phase estimate, and although being an effect common to the three methods, it may be enhanced in the new technique by the additional computations involved. Finally, the technique has been applied to a simulated velocity field and to a real dual-PRF velocity field with global aliasing, and verified that the methodology does not to generate false alarms and appropriately corrects the outliers in the boundaries of globally aliased areas.

Acknowledgments. The present work results from a brief but prolific research stay at the ANL in Illinois; we are sincerely grateful to the ARM Radar Group at the ANL for the hospitality and for their altruistic guidance and suggestions. We are also grateful to two anonymous reviewers, who have helped to improve the final form of this paper. The computations and algorithms described

in this manuscript have been implemented based on the Python ARM Radar Toolkit (Helmus and Collis 2016), an open-source Python module for weather radar data processing. This study and the research stay were co-funded by the autonomous Government of Catalonia and the Meteorological Service of Catalonia, under the framework of the Industrial Doctorate Programme (Project DI 14P/2012). This study is also included under the framework of the HyMeX program and was carried out with partial support from the Spanish Project CGL2015-65627-C3-2-R (MINECO/FEDER), with the University of Barcelona as recipient. The Argonne National Laboratory's work was supported by the U.S. Department of Energy (DOE), Office of Science, Office of Biological and Environmental Research (OBER), under Contract DE-AC02-06CH11357, with UChicago Argonne LLC as recipient of this Prime Contract. This work was supported by OBER of the DOE as part of the ARM program.

REFERENCES

Altube, P., J. Bech, O. Argemí, and T. Rigo, 2015: Quality control of antenna alignment and receiver calibration using the sun: Adaptation to midrange weather radar observations at low elevation angles. *J. Atmos. Oceanic Technol.*, **32**, 927–942, doi:10.1175/JTECH-D-14-00116.1.

Banjanin, Z. B., and D. S. Zrnić, 1991: Clutter rejection for Doppler weather radars which use staggered pulses. *IEEE Trans. Geosci. Remote Sens.*, **29**, 610–620, doi:10.1109/36.135823.

Bech, J., and Coauthors, 2004: The weather radar network of the Catalan Meteorological Service: Description and applications. *Third European Conference on Radar in Meteorology and Hydrology together with the COST 717 Final Seminar*, ERAD Publication Series, Vol. 2, ERAD, 416–420.

——, R. Pascual, T. Rigo, N. Pineda, J. M. López, J. Arús, and M. Gayà, 2007: An observational study of the 7 September 2005 Barcelona tornado outbreak. *Nat. Hazards Earth Syst. Sci.*, **7**, 129–139, doi:10.5194/nhess-7-129-2007.

——, and Coauthors, 2011: A Mediterranean nocturnal heavy rainfall and tornadic event. Part I: Overview, damage survey and radar analysis. *Atmos. Res.*, **100**, 621–637, doi:10.1016/j.atmosres.2010.12.024.

Bellon, A., and I. Zawadzki, 2003: A 9-year summary of radar characteristics of mesocyclonic storms and deep convection in southern Québec. *Atmos.–Ocean*, **41**, 99–120, doi:10.3137/ao.410201.

Bergen, W. R., and S. C. Albers, 1988: Two- and three-dimensional de-aliasing of Doppler radar velocities. *J. Atmos. Oceanic Technol.*, **5**, 305–319, doi:10.1175/1520-0426(1988)005<0305:TATDDA>2.0.CO;2.

Bharadwaj, N., V. Chandrasekar, and F. Junyent, 2010: Signal processing system for the CASA Integrated Project 1 radars. *J. Atmos. Oceanic Technol.*, **27**, 1440–1460, doi:10.1175/2010JTECHA1415.1.

Brown, R. A., and V. T. Wood, 2007: A guide for interpreting Doppler velocity patterns: Northern Hemisphere edition. 2nd ed. NOAA/NSSL, 55 pp.

Cho, J. Y. N., 2005: Multi-PRI signal processing for the terminal Doppler weather radar. Part II: Range–velocity ambiguity mitigation. *J. Atmos. Oceanic Technol.*, **22**, 1507–1519, doi:10.1175/JTECH1805.1.

Dazhang, T., S. G. Geotis, R. E. Passarelli Jr., A. L. Hansen, and C. L. Frush, 1984: Evaluation of an alternating-PRF method for extending the range of unambiguous Doppler velocity. Preprints, *22nd Conf. on Radar Meteorology*, Zurich, Switzerland, Amer. Meteor. Soc., 523–527.

Doviak, R. J., and D. S. Zrnić, 2006: *Doppler Radar and Weather Observations*. 2nd ed. Dover Publications, 592 pp.

Eilts, M. D., and S. D. Smith, 1990: Efficient dealiasing of Doppler velocities using local environment constrains. *J. Atmos. Oceanic Technol.*, **7**, 118–128, doi:10.1175/1520-0426(1990)007<0118:EDODVU>2.0.CO;2.

Fisher, N. I., 1993: *Statistical Analysis of Circular Data.* 1st ed. Cambridge University Press, 279 pp.

Frush, C., R. J. Doviak, M. Sachidananda, and D. S. Zrnić, 2002: Application of the SZ phase code to mitigate range–velocity ambiguities in weather radars. *J. Atmos. Oceanic Technol.*, **19**, 413–430, doi:10.1175/1520-0426(2002)019<0413:AOTSPC>2.0.CO;2.

Haase, G., and T. Landelius, 2004: Dealiasing of Doppler radar velocities using a torus mapping. *J. Atmos. Oceanic Technol.*, **21**, 1566–1573, doi:10.1175/1520-0426(2004)021<1566:DODRVU>2.0.CO;2.

Hampel, F. R., E. M. Ronchetti, P. J. Rousseeuw, and W. A. Stahel, 1986: *Robust Statistics: The Approach Based on Influence Functions*. 1st ed. John Wiley and Sons, 511 pp.

Helmus, J. J., and S. M. Collis, 2016: The Python ARM Radar Toolkit (Py-ART), a library for working with weather radar data in the Python programming language. *J. Open Res. Software*, **4**, p.e25, doi:10.5334/jors.119.

Hengstebeck, T., D. Heizenreder, and P. Joe, 2014: Detection of atmospheric rotation by means of the DWD radar network. *Proc. Eighth European Conf. on Radar Meteorology and Hydrology*, Garmisch-Partenkirchen, Germany, ERAD, NOW. P11. [Available online at http://www.pa.op.dlr.de/erad2014/programme/ExtendedAbstracts/196_Hengstebeck.pdf.]

Holleman, I., and H. Beekhuis, 2003: Analysis and correction of dual PRF velocity data. *J. Atmos. Oceanic Technol.*, **20**, 443–453, doi:10.1175/1520-0426(2003)20<443:AACODP>2.0.CO;2.

James, C. N., and R. A. J. Houze Jr., 2001: A real-time four-dimensional Doppler dealiasing scheme. *J. Atmos. Oceanic Technol.*, **18**, 1674–1683, doi:10.1175/1520-0426(2001)018<1674:ARTFDD>2.0.CO;2.

Jing, Z., and G. Wiener, 1993: Two-dimensional dealiasing of Doppler velocities. *J. Atmos. Oceanic Technol.*, **10**, 798–808, doi:10.1175/1520-0426(1993)010<0798:TDDODV>2.0.CO;2.

Joe, P., and P. T. May, 2003: Correction of dual PRF errors for operational weather radars. *J. Atmos. Oceanic Technol.*, **20**, 429–442, doi:10.1175/1520-0426(2003)20<429:CODPVE>2.0.CO;2.

Jorgensen, D. P., T. R. Shepherd, and A. S. Goldstein, 2000: A dual-pulse repetition frequency scheme for mitigating velocity ambiguities of the NOAA P-3 airborne Doppler radar. *J. Atmos. Oceanic Technol.*, **17**, 585–594, doi:10.1175/1520-0426(2000)017<0585:ADPRFS>2.0.CO;2.

May, P. T., 2001: Mesocyclone and microburst signature distortion with dual PRT radar. *J. Atmos. Oceanic Technol.*, **18**, 1229–1233, doi:10.1175/1520-0426(2001)018<1229:MAMSDW>2.0.CO;2.

Miller, L. J., C. G. Mohr, and A. J. Weinheimer, 1986: The simple rectification to Cartesian space of folded radial velocities from Doppler radar sampling. *J. Atmos. Oceanic Technol.*, **3**, 162–174, doi:10.1175/1520-0426(1986)003<0162:TSRTCS>2.0.CO;2.

Miller, M. L., V. Lakshmanan, and T. M. Smith, 2013: An automated method for depicting mesocyclone paths and intensities. *Wea. Forecasting*, **28**, 570–585, doi:10.1175/WAF-D-12-00065.1.

Mitchell, E. D. W., S. V. Vasiloff, G. J. Stumpf, A. Witt, M. D. Eilts, J. T. Johnson, and K. W. Thomas, 1998: The National Severe Storms Laboratory tornado detection algorithm. *Wea. Forecasting*, **13**, 352–366, doi:10.1175/1520-0434(1998)013<0352:TNSSLT>2.0.CO;2.

Pierce, C., A. Seed, S. P. Ballard, D. Simonin, and Z. Li, 2012: Nowcasting. *Doppler Radar Observations—Weather Radar, Wind Profiler, Ionospheric Radar, and other Advanced Applications*, J. Bech and J. L. Chau, Eds., InTech, 97–142, doi:10.5772/39054.

Pineda, N., J. Bech, T. Rigo, and J. Montanyà, 2011: A Mediterranean nocturnal heavy rainfall and tornadic event. Part II: Total lightning analysis. *Atmos. Res.*, **100**, 638–648, doi:10.1016/j.atmosres.2010.10.027.

Ray, P. S., and C. Ziegler, 1977: De-aliasing first-moment Doppler estimates. *J. Appl. Meteor.*, **16**, 563–564, doi:10.1175/1520-0450(1977)016<0563:DAFMDE>2.0.CO;2.

Roca-Sancho, J., M. Berenguer, and D. Sempere-Torres, 2014: An inverse method to retrieve 3D radar reflectivity composites. *J. Hydrol.*, **519**, 947–965, doi:10.1016/j.jhydrol.2014.07.039.

Sachidananda, M., and D. S. Zrnić, 1999: Systematic phase codes for resolving range overlaid signals in a Doppler weather radar. *J. Atmos. Oceanic Technol.*, **16**, 1351–1363, doi:10.1175/1520-0426(1999)016<1351:SPCFRR>2.0.CO;2.

——, and ——, 2000: Clutter filtering and spectral moment estimation for Doppler weather radars using staggered pulse repetition time (PRT). *J. Atmos. Oceanic Technol.*, **17**, 323–331, doi:10.1175/1520-0426(2000)017<0323:CFASME>2.0.CO;2.

Sirmans, D., D. Zrnić, and B. Bumgarner, 1976: Extension of maximum unambiguous Doppler velocity by use of two sampling rates. Preprints, *17th Conf. on Radar Meteorology*, Seattle, WA, Amer. Meteor. Soc., 23–28.

Smith, T. M., K. L. Elmore, and S. A. Dulin, 2004: A damaging downburst prediction and detection algorithm for the WSR-88D. *Wea. Forecasting*, **19**, 240–250, doi:10.1175/1520-0434(2004)019<0240:ADDPAD>2.0.CO;2.

Stensrud, D. J., and Coauthors, 2009: Convective-scale warn-on-forecast system: A vision for 2020. *Bull. Amer. Meteor. Soc.*, **90**, 1487–1499, doi:10.1175/2009BAMS2795.1.

Stumpf, G. J., A. Witt, E. D. Mitchell, P. L. Spencer, J. T. Johnson, M. D. Eilts, K. W. Thomas, and D. W. Burgess, 1998: The National Severe Storms Laboratory mesocyclone detection algorithm for the WSR-88D. *Wea. Forecasting*, **13**, 304–326, doi:10.1175/1520-0434(1998)013<0304:TNSSLM>2.0.CO;2.

Sun, J., and N. A. Crook, 2001: Real-time low-level wind and temperature analysis using single WSR-88D data. *Wea. Forecasting*, **16**, 117–132, doi:10.1175/1520-0434(2001)016<0117:RTLLWA>2.0.CO;2.

Tabary, P., F. Guibert, L. Perier, and J. Parent-du-Chatelet, 2006: An operational triple-PRT Doppler scheme for the French radar network. *J. Atmos. Oceanic Technol.*, **23**, 1645–1656, doi:10.1175/JTECH1923.1.

Torres, S. M., Y. F. Dubel, and D. S. Zrnić, 2004: Design, implementation, and demonstration of a staggered PRT algorithm for the WSR-88D. *J. Atmos. Oceanic Technol.*, **21**, 1389–1399, doi:10.1175/1520-0426(2004)021<1389:DIADOA>2.0.CO;2.

Vaisala, 2014: User's manual: Digital IF receiver/Doppler signal processor, RVP8. Vaisala Oyj Doc. M211321EN-D, 522 pp.

Wapler, K., T. Hengstebeck, and P. Groenemeijer, 2016: Mesocyclones in central Europe as seen by radar. *Atmos. Res.*, **168**, 112–120, doi:10.1016/j.atmosres.2015.08.023.

WMO, 2008: *Guide to Meteorological Instruments and Methods of Observation*. WMO Tech. Rep. 8, 7th ed. World Meteorological Organization, 681 pp.

Xu, Q., K. Nai, L. Wei, P. Zhang, S. Liu, and D. Parrish, 2011: A VAD-based dealiasing method for radar velocity data quality control. *J. Atmos. Oceanic Technol.*, **28**, 50–62, doi:10.1175/2010JTECHA1444.1.